SOIL SCIENCE ANNUAL
2025, 76(4), 216247

https://doi.org/10.37501/soilsa/216247

BY-NC-ND

Principal component analysis of soil thermal regimes in Luvisols on contrasting slopes in the Wieliczka Foothills, south Poland

Tomasz Zaleski[1*], Mateusz Suchanek[1], Mariusz Klimek[2], Monika Szkalarska-Łukasik[1]

[1] University of Agriculture in Krakow, Department of Soil Science and Agrophysics, al. Mickiewicza 21, 31-120, Kraków, Poland
[2] Jagiellonian University, Faculty of Geography and Geology, Institute of Geography and Spatial Management, ul. Gronostajowa 7, 30-387 Kraków, Poland, mariusz.klimek@uj.edu.pl

[*] Corresponding author: dr hab. inż. Tomasz Zaleski, prof URK, t.zaleski@urk.edu.pl, ORCID iD: https://orcid.org/0000-0002-9785-3784

Received: 2025-12-02
Accepted: 2025-12-30
Published online: 2025-12-30
Associated editor: Piotr Gajewski

Keywords:

Luvisols
Soil thermal profiles
Slope exposure
Microclimatic variability
Wieliczka Foothills

Abstract

Soil temperature profiles are key indicators of microclimatic conditions and subsurface energy fluxes, and they are strongly controlled by slope aspect. Despite their importance, quantitative assessments of how contrasting slope exposures influence soil thermal regimes remain limited. In this study, we applied principal component analysis to a multi-year soil temperature dataset collected at several depths on north- and south-facing profiles Fragic Albic Endostanic Luvisol (Cutanic, Siltic) (IUSS Working Group WRB, 2022) in the Wieliczka Foothills (Outer Carpathians). The soils exhibit a typical sequence of genetic horizons, including humic, eluvial, illuvial, and parent material layers. The profiles were located on north- and south-facing slopes, both with comparable inclinations of approximately 10–12°. Temperature was measured using 5TM moisture and temperature sensors, with data recorded by an EM50 data logger (Decagon Devices, USA). Measurements were collected from 2015 to 2019 at 10-minute intervals from five sensors installed at depths of 10, 20, 40, 60, and 80 cm. Principal component analysis of soil temperature profiles revealed two dominant sources of thermal variability. The first principal component captured the seasonal dynamics expressed as annual temperature cycles across soil depths on both slopes. The second component clearly differentiated between slopes, showing a persistent, year-round thermal advantage and greater heat storage below 0.6 m depth on the south-facing slope. These results demonstrate that soil thermal profiles effectively capture microclimatic variability governed by slope aspect and provide a robust framework for evaluating landscape-scale thermal heterogeneity.

1. Introduction

Soil is a key component of the local climate system, functioning both as a heat sink and a heat store. Soil temperature reflects the balance between energy inflow and outflow in a given environment (Seyfried et al., 2021). The soil temperature profile, which refers to the distribution of temperature with depth, captures both short-term fluctuations in solar radiation (such as daily and weather-related changes) and longer-term seasonal and multi-year processes (Fan et al., 2023). On a small scale, it describes interactions between the atmosphere and the subsoil, while on a larger scale, it reflects regional climate, terrain exposure, and soil physical properties. The main factor determining the soil's thermal regime is the total amount of solar radiation (insolation) reaching the Earth's surface, which depends on global variables such as latitude, season, and average cloud cover (Hoyt, 1978; Bokwa and Skwera, 2008; Antonanzas-Torres et al., 2019; Bokwa at al. 2013; Bokwa et al. 2021), as well as local factors including relief, slope inclination and aspect, vegetation cover, organic matter, and particular soil properties such: mineral composition, texture, porosity, water content (Fan et al., 2019; Clouter et al., 2026).

Slope aspect is one of the primary factors that shape the microclimate (Eisenlohr et al., 2013). In southern Poland, as in other temperate zones of the Northern Hemisphere, south-facing slopes (SS, ang. south slope) receive significantly greater solar radiation throughout the year, while north-facing slopes (NS, ang. north slope) remain shaded for much of the year. These differences result in persistent variations in radiation balance, moisture content, and thermal conductivity of the subsoil, which consequently translate into distinct soil temperature profiles (Singh, 2018; Liang et al., 2024).

This study aims to provide a comprehensive, quantitative analysis of microclimatic differences between the north- and south-facing slopes of the Wieliczka Foothills, based on several years of monitoring of the soil profile temperature data. Principal component analysis (PCA) was employed to reduce the multidimensional dataset to a few key components for

© 2025 by the authors. Licensee Soil Science Society of Poland. This article is an open access article distributed under the terms and conditions of the Creative Commons Attribution (CC BY NC ND 4.0) license (https://creativecommons.org/licenses/by-nc-nd/4.0/).

interpretation. PCA has previously been used to summarise physical and chemical soil properties by location (Abdel-Fattah, 2020), identify important indicators of soil fertility (Hammad et al., 2025), and differentiate sensory characteristics of crops based on cultivation site (Rosenfeld et al., 1998). By comparing two sites with contrasting microclimates but similar soils, this study aims to provide a statistically robust and physically meaningful assessment of quantitative microclimatic differences.

2. Materials and methods

2.1. Location and soil characteristics

Soil temperature measurements were carried out at the Field Station of the Institute of Geography and Spatial Management, Jagiellonian University, situated in the village of Łazy at an elevation of 245 m above sea level. The village lies in the central part of the Małopolska Voivodeship, within the Rzezawa commune, and forms part of the transitional zone between the Wieliczka Foothills and the Sandomierz Basin. The study was conducted on soils developed from loess-like deposits in Carpathian Foothills (Zasoński, 1979; Zasoński, 1981; Gerlach et al., 1993; Szymański et al., 2011; Zaleski, 2012). According to the WRB classification (IUSS Working Group WRB, 2022), these soils were classified as Albic Endostanic Luvisol (Cutanic, Siltic) (IUSS Working Group WRB, 2022). The soil cover is characterised by high porosity, a low clay fraction, and a relatively loose, capillary structure. Hydrophysical and physical analyses of these soils indicate that the silty parent material is characterised by high water-holding capacity, while hydraulic conductivity varies depending on the arrangement of genetic horizons, particularly the depth and properties of the eluvial, illuvial and argic horizons (Zaleski, 2009; Zaleski, 2012; Dziczek et al. 2025). This is due to the predominance of medium-sized and fine-grained pores, as well as variable degrees of compaction, particularly in surface layers subject to erosion and deflation (Skiba, 1995; Zaleski et al., 2003; Zaleski, 2012). The soils have a silty clayey texture throughout all horizons. The organic matter content in the upper 20 cm ranges from 12.54 to 7.85 $g \cdot kg^{-1}$, while bulk density varies with depth (Table 1).

The soils were located on NS (N 49°58’03.7” E 20°29’32.2”) and SS (N 49°57’56.6” E 20°29’42.3”), both exhibiting comparable inclinations of approximately 10°–12°. The soils exhibit a typical sequence of genetic horizons: humic, eluvial, illuvial, and parent material. The analyses included determination of particle-size distribution according to PN-R-04032 (1998), with the sand fraction (2.0–0.05 mm) separated by wet sieving and classified following the guidelines of the Polish Society of Soil Science, organic carbon content (Corg.) determined using the Tiurin method, modified by Oleksynowa (Oleksynowa et al., 1993), and bulk density determined using 100 cm^3 core cylinders (Blake and Hartge, 1986).

2.2. Measurement technique

The Fig. 1 depicts the monitoring system, showing (a) Decagon EM50B data logger (Decagon Devices USA) connected to (b) a set of five 5TM soil moisture and temperature sensors. This is a professional soil monitoring system, with the measurements analysed in this paper focusing on temperature. The logger features an independent power supply (five AA batteries), ensuring continuous operation for several months and making it suitable for long-term outdoor use. The manufacturer states that the absolute accuracy of the temperature measurement is ±1°C, and practice indicates that the relative accuracy between sensors is comparable to a resolution of 0.1°C.

Table 1
Properties of the investigated soils

Soil horizon	Depth [cm]	C organic [$g \cdot kg^{-1}$]	% fraction in diameter in mm			Bulk density [$Mg \cdot m^{-3}$]
			2,0–0,05	0,05–0,002	<0,002	
Soil S						
A	0–22	10.5	24	68	8	1.499
Et	22–43	6.4	19	73	8	1.546
EB	43–58		19	69	12	1.685
Bt	58–93		23	64	13	1.707
BC	93–126		25	63	12	1.727
C	126–155		22	66	12	1.717
Soil N						
A	0–25	12.54	21	68	11	1.36
Et	25–48	7.85	19	72	9	1.53
EB	48–62		17	72	11	1.45
Bt	62–88		19	66	15	1.59
BC	88–121		18	64	18	1.62
C	121–150		20	66	14	1.72

a

b

Fig. 1. The soil temperature measurement system: (a) Decagon EM50 data logger and (b) temperature measurement probes installed in the soil profile on the south-facing slope

The sensors, permanently connected by cables, were buried on both north- and south-facing slopes at a turfed, regularly mowed site. The measurement period spanned four full years, from January 1, 2015, to January 1, 2019. During this time, data were collected at 10-minute intervals from sensors positioned at depths of 10, 20, 40, 60, and 80 cm.

2.3. Data analysis

Due to the use of unattended digital sensors in challenging environments, the data were subject to random digital noise, such as occasional incorrect sign or digit values (e.g., 0.4 instead of 2.4, or –0.4 instead of 0.4). To address this, the measurements were first filtered to remove such distortions using a spike detection algorithm. This algorithm calculates the absolute difference between consecutive measurements (T[i] – T[i-1]) and compares it to a predefined maximum allowable change. If the difference exceeds this threshold, the current value is considered an anomaly and is replaced with the previous valid measurement. Based on data review, the maximum permissible temperature changes in a 10-minute interval were set as follows: for depths of 0.8 m and 0.6 m, no more than 0.1°C; for 0.4 m, 0.2°C; for 0.2 m, 0.4°C; and for 0.1 m, 1.0°C.

Before the targeted statistical analysis, a set of features was selected to characterise the studied habitats. These features encompass a variety of physical information, including thermal levels, circadian cycle intensity and dominance, heat fluxes, thermal stability, thermal wave propagation, heat attenuation, and responses to sunrise and sunset (Sanford et al., 2024). The proposed set of features is also statistically diverse in scale, characteristics, and structure, thanks to the very dense data collection, every 10 minutes over 4 years:

Features 1–5. Monthly mean temperature (T_{month}) at each depth:

$$T_{month} = \frac{\sum_k T_k}{k},$$

where k is the number of measurements within a given month.

Features 6–10. Monthly mean daily temperature amplitude (A_T) at each depth:

$$A_T = \frac{\sum_j \left(T_{\max\,(24h)} - T_{\min\,(24h)}\right)_j}{j},$$

where j is the number of days in the month.

These features quantify the intensity of daily thermal fluctuations at different depths, indicating how deeply daily cycles propagate into the soil.

Features 11–14. Vertical temperature gradients (G), are defined as differences in monthly mean temperatures between adjacent depths (upper ($d1$) minus lower ($d2$)):

$$G_{d1,d2} = \frac{\sum_j \left(\overline{T}_{month(d1)}\right)_j}{j} - \frac{\sum_j \left(\overline{T}_{month(d2)}\right)_j}{j},$$

where j is the number of days in the month.

These gradients characterise the direction and magnitude of heat flow in the soil.

Features 15–19: Monthly mean daily temperature variability, defined as daily temperature standard deviation (STD), averaged over each month and depth:

$$STD_T = \frac{\sum_j (std(T_{24h}))_j}{j},$$

where *j* is the number of days in the month.

These features describe short-term temperature fluctuations independently of the monthly mean temperature level.

Feature 20: Phase lag (*R*) of the thermal wave.

The phase lag determines the time lag between temperature changes observed in the shallow layer (0.1 m) reaching the deeper layer (0.8 m). This reflects the speed of heat wave propagation in the soil profile. This characteristic is calculated as the time shift τ, for which the cross-correlation between monthly temperature signals from both depths reaches its maximum value:

$$R(\tau) = Corr(T_{0.1m}(t), T_{0.8m}(t+\tau).$$

The lag corresponding to the maximum correlation is converted into days:

$$lag_{(0.1-0.8)} = argmax_\tau \cdot R(\tau) \cdot \Delta t_{days},$$

where $argmax_\tau \cdot R(\tau)$ represents the sample shift at maximum correlation, and Δt_{days} converts the sampling interval (10 minutes) into days.

Feature 21: Attenuation of daily amplitude with depth:

$$attenuation = \ln\left(A_{0.1m(24h)}\right) - \ln\left(A_{0.8m(24h)}\right).$$

Amplitude attenuation refers to the degree to which the daily temperature amplitude decreases with depth.

Features 22: Power of the daily frequency component (*DPR*).

This feature indicates the strength of the 24-hour rhythm in the monthly temperature signal at a depth of 0.1 m, i.e., the extent to which the monthly temperature record is dominated by the day-night cycle. To this end, a frequency spectrum is determined from the monthly temperature data using a fast Fourier transform (FFT). The spectral power corresponding to the diurnal frequency (1/24 h) is then normalised to the total spectral power for the given month:

$$DPR = \frac{P(f = 1/day)}{\sum_f P(f)}.$$

Feature 23: Morning heating rate (HR).

The monthly value of this feature is determined as the average daily temperature increase rate at a depth of 0.1 m, calculated over the standard time window of 04:00–08:00.

$$HR = \frac{\sum_j \left(\frac{T(t=8{:}00) - T(t=4{:}00)}{\Delta t_{hours}}\right)_j}{j},$$

where *j* is the number of days in the month.

This feature can be interpreted as an indicator of the dynamics of morning solar energy input and the surface soil layer's responsiveness to heating.

Feature 24: Evening cooling rate (*CR*).

The rate of surface cooling during the evening hours due to heat loss from the surface layer through radiation and conduction into the profile. The monthly *CR* is defined as the average daily temperature decrease at 0.1 m during the period 18:00–22:00.

$$CR = \frac{\sum_j \left(\frac{T(t=18{:}00) - T(t=22{:}00)}{\Delta t_{hours}}\right)_j}{j},$$

where *j* is the number of days in the month.

This feature reflects the effectiveness of evening radiative cooling and the rate at which the surface soil layer releases heat.

This approach resulted in a comprehensive dataset with well-defined physical meaning. Principal component analysis (PCA) was then applied to extract the most significant features differentiating the slopes and to facilitate visualisation. All calculations and figures were produced using Python 3.10 with the NumPy, Pandas, SciPy, scikit-learn, and Matplotlib libraries.

3. Results and discussion

3.1. Interpretation of the first principal component (PC1) – the seasonality component

Based on soil temperature measurements collected from January 1, 2015, to January 1, 2019, a set of 24 features was calculated and subsequently subjected to PCA. This procedure transformed the original feature set into a new orthogonal component space, in which the first three principal components (PC1, PC2, PC3) explain nearly all of the variance in the data. Notably, PC1 and PC2 together account for more than 80% of the total variability, capturing the dominant structure of thermal dynamics within the soil profile. Therefore, the interpretation and graphical presentation in this study focus exclusively on the PC1–PC2 component space.

PC1 reflects the dominant seasonal signal present in the data. As shown in Fig. 2, PC1 values exhibit a clearly cyclical pattern over time, reaching their minimum in winter, increasing during spring, attaining their highest values in summer, and then gradually declining throughout autumn. This regularity suggests that PC1 serves as a synthetic indicator of seasonal changes in the soil profile's thermal conditions, driven by the annual cycle of solar insolation.

The largest contribution to PC1 comes from variables with the highest absolute loadings, which represent the absolute temperature level and the overall thermal activity of the soil profile. The strongest loadings are associated with (i) mean monthly temperatures in the shallow and intermediate layers ($T_{month(0.2\,m)}$ 0.2888, ($T_{month(0.1\,m)}$ 0.2886, ($T_{month(0.4\,m)}$ 0.2831)

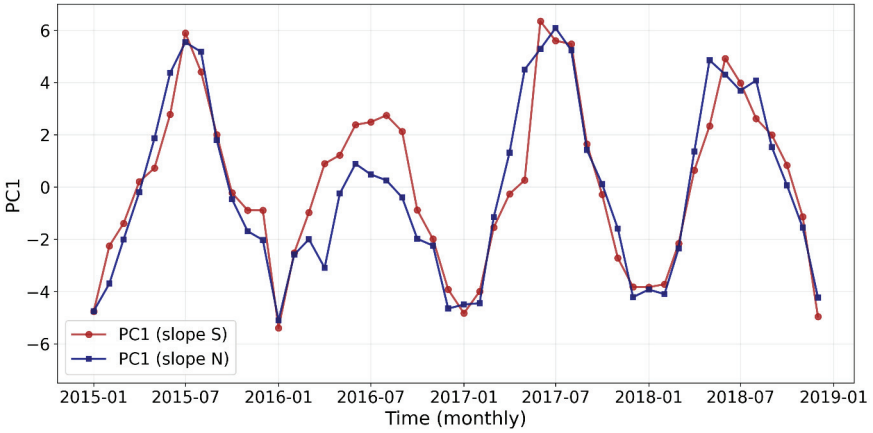

Fig. 2. Average values of the first principal component (PC1) of soil temperature for both soils (slopes) for the period from January 1, 2015, to January 1, 2019

and (ii) metrics of daily thermal dynamics in the surface layer, including daily temperature amplitude and standard deviation ($A_{T(0.1\,m)}$ 0.2831, ($STD_{T(0.1\,m)}$ 0.2830, respectively). These features respond most strongly to seasonal changes in solar energy input: in summer, higher temperatures, greater daily amplitudes, and greater daily-average thermal variations increase PC1, while in winter, the opposite is observed.

Thus, PC1 can be interpreted as an index of soil thermal seasonality, reflecting the combined effects of changes in solar radiation, atmospheric conditions, and soil properties. The cyclic pattern is identical for both slopes, indicating that the sites experience the same global climate and that the soils on both slopes store and conduct heat similarly in response to seasonal energy fluxes. Therefore, the soils on both slopes exhibit similar thermal properties.

3.2. Interpretation of the second principal component (PC2) – microclimatic component

The Fig. 3 presents the values of the second principal component (PC2) as a function of time. PC2 provides a clear and stable separation of data from the south slope and the north slope. Throughout the observation period, PC2 values remained systematically higher (positive) for the NS and lower (negative) for the SS (Fig. 3). This indicates that PC2 serves as an index of microclimatic differences between slopes with different exposure to solar radiation.

To understand the physical significance of the obtained separation, the structure of the PC2 component loadings was also analysed. Ranking the loading values shows that the largest contribution to PC2 comes from the average monthly temperatures of the deepest soil layers ($T_{month(0.6\,m)}$ 0.419, ($T_{month(0.8\,m)}$ 0.405), as well as the temperature gradients in the outermost layers (the lower gradient between 0.6 m and 0.8 m ($GD_{(0.6\,m-0.8\,m)}$ 0.395) and the upper gradient between 0.1 m and 0.2 m ($GD_{(0.1\,m-0.2\,m)}$ 0.328). These are therefore the features that most differentiate the slopes.

The deepest soil layers significantly differentiate the thermal profiles of the studied slopes, generating signals that are devoid of diurnal, weather, or random variations. The average monthly temperatures at depths of 0.6 m and 0.8 m reflect the long-term energy balance of the soil, which is directly related to

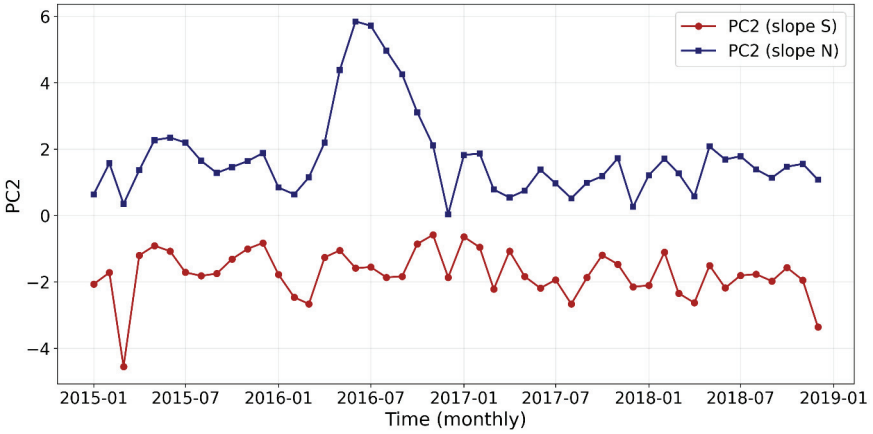

Fig. 3. Second principal component (PC2) of soil temperature for the NS (blue) and SS (red) slopes for the period from January 1, 2015, to January 1, 2019

long-term radiation, heat absorption, and the direction of heat flow. Throughout the entire observation period, the deeper soil on the southern slope remains systematically warmer, indicating a persistent thermal advantage associated with higher long-term solar exposure.

Temperature gradients provide information about the intensity and direction of heat flow. The gradient between the shallowest layers (0.1 m–0.2 m) and the deepest layers (0.6 m–0.8 m) strongly differentiates the slopes, while the gradient of the middle layers (0.4–0.6 m) has little effect, as its loading is close to zero. This is because the mechanisms responsible for gradient differentiation differ by depth. Near the surface, large differences in the temperature gradient between slopes are most visible in autumn and winter, when the southern slope responds dynamically to insolation, while the NS responds little or not at all (Fig. 3). This is a short-term effect related to diurnal and seasonal solar radiation variability. In contrast, the deepest layers do not respond to short-term fluctuations but reflect the cumulative heat accumulated over many weeks or months, with the SS storing more heat at depth due to greater solar energy input. The central gradient (0.4 m–0.6 m) does not differentiate the slopes because this layer lies between two zones with different thermal regimes; its temperature is influenced by both short-term and long-term processes, making it similar on both slopes and thus not an effective separating feature in PCA.

The Fig. 4 shows the data in the space of the first two principal components (PC1 and PC2), which together explain most of the thermal variability of the soil profile. The data in Fig. 4a form a closed annual loop. Points corresponding to the winter months (saturated colours) are concentrated on the left side of the graph (low PC1, low system energy). They then move to the right side of the graph towards positive PC1 values during the spring and summer months, before returning to winter levels in the fall. Observing this trajectory confirms that PC1 represents a global seasonal signal. Only when we group the points according to the slopes, as in Fig. 4b, do we obtain full separation on the PC2 axis: circle points with negative PC2 values correspond to the SS and reveal a warmer profile with strong heat flux into the interior; square points with positive PC2 values correspond to the SN slope and reveal a cooler, less solar-intensive profile. It is worth emphasising that these differences are present systematically throughout the year; even in winter, the SS stores more energy. This finding indicates that the thermal profile of Luvisol can serve as a sensitive microclimate indicator related to energy balance and the direction of heat flow. The graph also reveals asymmetry in the point cloud. The smallest separation between slopes occurs in winter. Differences are preserved because the southern slope retains heat in deeper layers (summer thermal memory), while the northern slope loses heat more quickly. However, the SS surface warms slowly in winter, the diurnal signal disappears, and snow cover (if present) can act as an insulator. These processes result in the smallest slope differentiation during this period. In early spring, both slopes remain cold, and increased meltwater can enhance thermal conductivity similarly. As the year progresses, differences increase, with the greatest separation observed in late spring and summer, when the SS absorbs and stores more energy at depth due to maximum insolation. During autumn, the SS continues to absorb heat (not as intensely as in summer), but the NS enters a cooling phase in which radiative processes begin to dominate solar absorption. During this period, there is still significant separation between the slopes relative to PC2.

To quantitatively assess how well individual features are represented by PCA, communality coefficients were calculated for the first two principal components (PC1 and PC2) and are presented in Table 2. Communality indicates the proportion of variance in a given feature that is jointly explained by PC1 and PC2. Analysis of the communality coefficients showed that PC1 and PC2 account for the greatest portion of variability in features associated with the deeper part of the soil profile. The highest communality values (approximately 15–18%) were observed for mean monthly temperatures at depths of 0.6 and 0.8 m, as well as for the temperature gradient between these layers, highlighting the dominant role of long-term energy balance in slope differentiation. Near-surface features, such as temperature amplitude, diurnal variability, and the gradient between 0.1 and 0.2 m, exhibit moderate communality (approximately 10–12%), reflecting the influence of short-term radiative processes. For the remaining features, the communality systematically decreases, confirming that PCA effectively separates the seasonal component from microclimatic variability, focusing on the most stable and physically significant processes.

The qualitative results obtained in this study are consistent with recent research highlighting the role of soil temperature in reflecting local and regional microclimates. For example, Kunkel et al. (2015) analysed soil temperature dynamics at the scale of large catchments (500–1000 km^2) and demonstrated a strong influence of slope orientation on soil temperature due to differences in solar radiation. However, they also showed that terrain shading (e.g. forest cover) can weaken this relationship, as the actual incoming radiation is lower than the theoretical potential. Based on deep borehole measurements in the Czech part of the Krusznych Mountains, Šafanda et. al. (1999) extrapolated mean annual ground surface temperatures and found that variability driven solely by slope aspect can reach up to 1.1°C. Wundram et. al. (2010) demonstrated in alpine environments that locally induced soil temperature gradients in the upper soil layer (0–15 cm), related to topography (e.g. north- versus south-facing slopes), can outweigh the general altitudinal temperature gradient during specific times of day and seasons. The present study refers to a temperate climate of the Northern Hemisphere, where, similarly to Mostowik et. al. (2023), a clear and persistent relationship between soil temperature and slope exposure was observed throughout the year. In contrast, studies from subtropical regions (Xu et. al., 2025) indicate that during the rainy season, the influence of slope aspect on soil temperature may diminish, reflecting the dominant role of moisture and cloud cover. These findings support the conclusion that Luvisol thermal profiles are sensitive recorders of both the dominant regional seasonal signal and the superimposed local effects arising from slope exposure.

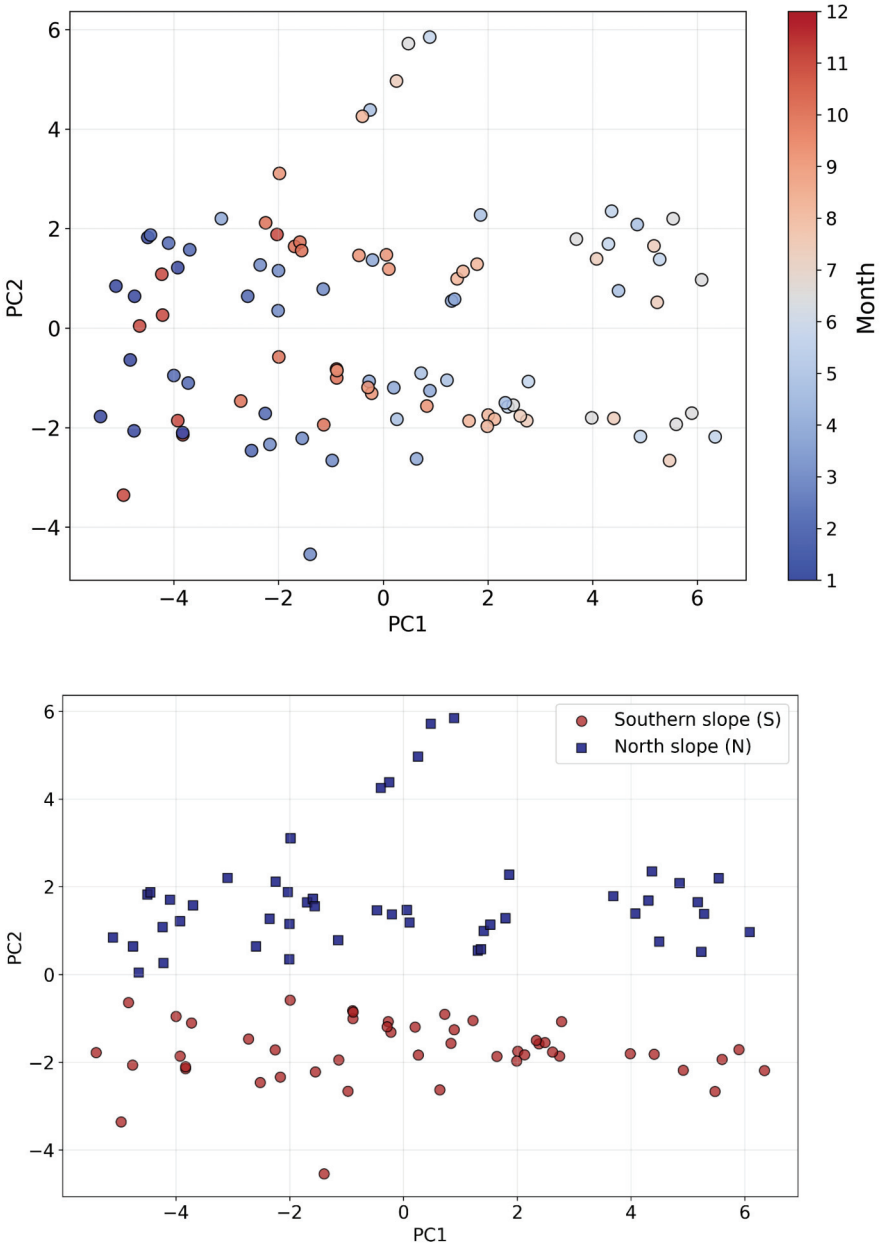

Fig. 4. Principal component analysis (PCA) results for the first (PC1) and second (PC2) components, showing (a) the seasonal trajectory of environmental conditions coloured by sampling month (from January (saturated blue) to December (saturated red)) and (b) the separation of microclimatic conditions between southern and northern slopes along PC2

Table 2
Dominant loadings and communality coefficients for variables in PC1 and PC2

Feature	Loading PC1	Loading PC2	Communality [%]
T_{month} (0.6 m)	0.050	0.419	17.8
T_{month} (0.8 m)	0.081	0.405	17.1
G (0.6 m, 0.8 m)	0.014	0.395	15.6
A_T (0.2 m)	0.256	–0.240	12.3
STD_T (0.2 m)	0.256	–0.239	12.2
G (0.1 m, 0.2 m)	0.041	0.328	11.0

4. Conclusions

The results of this study, supported by principal component analysis, demonstrate that PC1 and PC2 collectively capture the integration of regional and local controls on the thermal regime of Luvisols. The physical variables that most strongly determine PC1 are the mean monthly temperatures at depths of 0.1 m, 0.2 m, and 0.4 m, as well as the daily amplitude and variability of surface temperature (0.1 m). The temporal evolution of these features (i.e., their annual cycle) is very similar on both slopes. PC1 is a stable indicator of thermal seasonality, encapsulating the cyclical progression from cold, low-energy winter conditions to warm, high-energy summer states and the subsequent return to autumnal cooling. In turn, the physical variables that most strongly determine PC2 are the mean monthly temperatures at depths of 0.6 m and 0.8 m, as well as the thermal gradients in the shallowest and deepest soil layers. The temporal evolution of these features is fundamentally different on the two slopes. PC2 represents an index of aspect-driven microclimatic differentiation, expressing the persistent, year-round thermal advantage of the southern slope in the deeper soil layers (beyond 60 cm), along with the associated contrasts in heat storage and heat-flow direction. Together, PC1 and PC2 demonstrate that Luvisol thermal profiles are sensitive indicators of both the dominant regional seasonal signal and the superimposed local effects resulting from slope exposure.

Acknowledgements

This research was conducted with the support of the Ministry of Science and Higher Education.

Conflict of interest

The authors declare that they have no conflict of interest. The authors declare that they have no known competing financial interests or personal relationships that could have appeared to influence the work reported in this paper. This research did not involve human or animal subjects.

Author Contributions

Mateusz Suchanek – Methodology, Data analysis, Visualisation, Writing – original draft. **Mariusz Klimek** – Data curation, Field Investigation. **Monika Szklarska-Łukasik** – Data curation, Writing – original draft. **Tomasz Zaleski** – Conceptualisation, Data curation, Funding acquisition, Investigation, Methodology, Data analysis, Supervision, Validation, Visualisation, Writing – original draft, Writing – review & editing. All authors read and approved the final manuscript.

References

Abdel-Fattah, M.K., 2020. A GIS-based approach to identify the spatial variability of salt affected soil properties and delineation of site-specific management zones: a case study from Egypt. Soil Science Annual 71(1), 76–85. https://doi.org/10.37501/soilsa/121495

Antonanzas-Torres, F., Urraca, R., Polo, J., Perpinan-Lamigueiro, O., Escobar, R., 2019. Clear sky solar irradiance models: a review of seventy models. Renewable and Sustainable Energy Reviews 107, 374–387. https://doi.org/10.1016/J.RSER.2019.02.032

Blake, G.K., Hartge, K.H., 1986. Methods of Soil Analysis. Part 1. Bulk Density. In: A. Klute, ed. Agronomy Monograph 9(1), pp. 363–375. Madison, USA, American Society of Agronomy (ASA).

Bokwa, A., Skwera, B., 2008. Relief and land use impact on the atmospheric precipitation structure in Cracow's surroundings (1971–2005). Infrastructure and Ecology of Rural Areas 5(05), 51–61. (in Polish with English summary).

Bokwa, A., Klimek, M., Krzaklewski, P., Kukułka, W., 2021. Drought Trends in the Polish Carpathian Mts. in the Years 1991–2020. Atmosphere 12, 1259. https://doi.org/10.3390/atmos12101259

Bokwa, A., Wypych, A., Ustrnul, Z., 2013. Climate Changes in the Vertical Zones of the Polish Carpathian in the Last 50 Years. In The Carpathians: Integrating Nature and Society towards Sustainability; Kozak, J., Ostapowicz, K., Bytnerowicz, A., Wyżga, B., Eds.; Springer: Berlin/Heidelberg, Germany, pp. 89–110.

Clouter, S., González-Pinzon, R., Schoener, G., 2026. Effects of Slope, Compaction, Gravel Mulch, and Landscape Fabric on Infiltration for Sandy Soils. Journal of Hydrologic Engineering 31(1). https://doi.org/10.1061/JHYEFF.HEENG-6639

Dziczek, J., Sykuła, M., Świtoniak, M., 2025. The impact of erosion on the spatial variability of main properties, genesis, and systematic position of soils in the Wieliczka Foothills, southern Poland – a case study from the Bemke Campus area. Soil Science Annual 76(3), 209899. https://doi.org/10.37501/soilsa/209899.

Eisenlohr, P.V., Alves, L.F., Bernacci, L.C. et al., 2013. Disturbances, elevation, topography and spatial proximity drive vegetation patterns along an altitudinal gradient of a top biodiversity hotspot. Biodiversity Conservation 22, 2767–2783. https://doi.org/10.1007/s10531-013-0553-x

Fan, X., Li, W., Wu, X., Yao, M., Niu, F., Lin, Z., 2023. Heterogeneity of Surface Heat Exchange of Slopes and Potential Drivers of the Initiation of Thaw Slump, Qinghai-Tibet Plateau. International Journal of Disaster Risk Science 14, 549–565. https://doi.org/10.1007/s13753-023-00508-8

Fan, Y., Clark, M., Lawrence, D.M., Swenson, S., Band, L.E., Brantley, et al., 2019. Hillslope Hydrology in Global Change Research and Earth System Modelling. Water Resources Research 55(2), 1737–1772. https://doi.org/10.1029/2018WR023903

Gerlach, T., Krysowska-Iwaszkiewicz, M., Szczepanek, K., Pazdur, M.F., 1993. New data on the cover of the Carpathian variety of loesses in Humniska near Brzozów. Zeszyty IGiPZ PAN 16, 1–43. (in Polish with English summary)

Hammad, J.A., M'nassri, S., Chaabane, B., Al Bayati, A.-H.I., Majdoub, R., 2025. High-resolution baseline digital mapping of soil fertility in the Euphrates basin, western Iraq. Soil Science Annual 76(3), 207765. https://doi.org/10.37501/soilsa/207765

Hoyt, D.V., 1978. A model for the calculation of solar global insolation. Solar Energy 21(1), 27–35. https://doi.org/10.1016/0038-092X(78)90113-5

IUSS Working Group WRB, 2022. World Reference Base for Soil Resources. International soil classification system for naming soils and creating legends for soil maps. 4th edition. International Union of Soil Sciences (IUSS), Vienna, Austria.

16. Kunkel, V., Wells, T., Hancock, GR., 2016. Soil temperature dynamics at the catchment scale. Geoderma 273, 32–44. https://doi.org/10.1016/j.geoderma.2016.03.011

Liang, T., Tian, F., Zou, L., Jin, H., Tagesson, T., Rumpf, S., He, T., Liang, S., Fensholt, R., 2024. Global assessment of vegetation patterns along topographic gradients. International Journal of Digital Earth 17(1), 1–19. https://doi.org/10.1080/17538947.2024.2404232

Mostowik, K., Kafel, A., Kisiel, M., Kozioł, A., Paruch, D., Płaczkowska, E., Rzonca, B., Siwek, J., Słotwiński, J., Stolarczyk, M., 2023. The variability of soil temperature and moisture across the Połonina Wetlińska

Range (the Western Bieszczady Mountains). Prace Geograficzne 173 57–85. https://doi.org/10.4467/20833113PG.23.019.19231 (in Polish with English abstract)

Oleksynowa, K., Tokaj, J., Jakubiec, J., Komornicki, T., 1993. Guide to exercises in soil science and geology. Part II. Laboratory methods of soil analysis (in Polish). Agricultural University of Krakow, pp. 134.

PN-R-04032: 1998. Soils and mineral materials – Sampling and determination of particle-size distribution (in Polish).

Rosenfeld, H.J., Samuelsen, R.T., Lea, P., 1998. The effect of temperature on sensory quality, chemical composition and growth of carrots (Daucus carota L.) I. Constant diurnal temperaturę. The Journal of Horticultural Science and Biotechnology 73(2), 275–288. https://doi.org/10.1080/14620316.1998.11510975

Šafanda, J., 1999. Ground surface temperature as a function of slope angle and slope orientation and its effect on the subsurface temperature field. Tectonophysics 306(3–4), 367–375. https://doi.org/10.1016/S0040-1951(99)00066-9

Sanford, R., Chee-Sanford, J.C., Yang W.H., 2024. Diurnal temperature variation in surface soils: an underappreciated control on microbial processes. Frontiers in Microbiology 15. https://doi.org/10.3389/fmicb.2024.1423984

Seyfried, M., Flerchinger, G., Bryden, S., Link, T., Marks, D., McNamara, J., 2021. Slope and Aspect Controls on Soil Climate: Field Documentation and Implications for Large-scale Simulation of Critical Zone Processes. Vadose Zone Journal 20, e20158. https://doi.org/10.1002/vzj2.20158.

Singh, S., 2018. Understanding the role of slope aspect in shaping the vegetation attributes and soil properties in Montane ecosystems. Tropical Ecology 59(3), 417–430.

Skiba, S., 1995. Soil Cover. [In:] Warszyńska, J. (Ed.), The Polish Carpathians. Nature, Man, and His Activities. Jagiellonian University, Krakow, 69–76. (in Polish)

Szymański, W., Skiba, M., Skiba, S., 2011. Fragipan horizon degradation and bleachedtongues formation in Albeluvisols of the Carpathian Foothills, Poland. Geoderma 167–168, 340–350. https://doi.org/10.1016/j.geoderma.2011.07.007

Wundram, D., Pape, R., Löffler, J., 2010. Alpine Soil Temperature Variability at Multiple Scales, Arctic, Antarctic, and Alpine Research 42(1), 117–128. https://doi.org/10.1657/1938-4246-42.1.117

Xu, J., Liu, M., Mei, S., Yang, Q., Zhang, J., Yi, J., Ding, S., Tan, Y., 2025. Characteristics and controlling factors of soil micro-climate in a subtropical re-vegetation catchment: Insights from continuous moisture and temperature observations. Plant and Soil. https://doi.org/10.1007/s11104-025-08131-w

Zaleski, T., Klimek, M., Głąb, T., 2003. The comparison of penetration resistance of lessive soils in different land use of the Wieliczka Foothills. Advances of Agricultural Sciences Problem Issues 493, 555–562. (in Polish with English summary)

Zaleski, T., 2009. Pedogenetic conditions affecting hydrophysical properties of Luvisols derived from loess. Folia Geographica 40, 83–94.

Zaleski, T., 2012. The role of pedogenesis in shaping the hydrophysical properties, water retention, water regime and water balance of soils derived from silty deposits of the Carpathians. Wydawnictwo Uniwersytetu Rolniczego, Kraków 494, (371), University of Agriculture in Krakow, pp. 114. (in Polish with English summary)

Zasoński, S., 1979. Właściwości mikromorfologiczne a główne procesy glebotwórcze niektórych gleb Pogórza Wielickiego. Roczniki Gleboznawcze – Soil Science Annual 30(2), 163–184. (in Polish with English abstract)

Zasoński, S., 1981. Main soil-forming processes on loess-derived materials in the Wieliczka Foothills. Part I. General characteristics of soils and selected chemical properties. Roczniki Gleboznawcze – Soil Science Annual 32(2), 115–143. (in Polish with English abstract)

Analiza głównych składowych właściwości termicznych gleb płowych na stokach o przeciwnej ekspozycji na Pogórzu Wielickim

Słowa kluczowe:

Gleby płowe
Profile termiczne gleby
Ekspozycja stoków
Zmienność mikroklimatyczna
Pogórze Wielickie

Streszczenie

Profile temperatury gleby są kluczowymi wskaźnikami warunków mikroklimatycznych i podziemnych przepływów energii, a ich wpływ jest silnie zależny od ekspozycji stoków. Pomimo ich znaczenia, ilościowe oceny wpływu kontrastujących ekspozycji stoków na reżimy termiczne gleby pozostają ograniczone. W niniejszym badaniu zastosowaliśmy analizę głównych składowych (PCA) do wieloletniego zbioru danych dotyczących temperatury gleby zebranych na kilku głębokościach w dwóch profilach gleb płowych o ekspozycji północnej i południowej (WRB 2022) na Pogórzu Wielickim (Karpaty Zewnętrzne). Gleby te charakteryzują się typową sekwencją poziomów genetycznych, obejmującą warstwy próchniczne, eluwialne, iluwialne i materiału macierzystego. Profile zlokalizowano na stokach o ekspozycji północnej i południowej, o porównywalnym nachyleniu około 10–12°C. Temperaturę mierzono za pomocą czujników wilgotności i temperatury 5TM, a dane rejestrowano za pomocą rejestratora danych EM50 (Decagon Devices, USA). Pomiary wykonywano w latach 2015–2019 w odstępach 10-minutowych za pomocą pięciu czujników zainstalowanych na głębokościach 10, 20, 40, 60 i 80 cm. Analiza głównych składowych profili temperatury gleb wykazała istnienie dwóch dominujących źródeł zmienności termicznej. Pierwsza składowa główna odzwierciedlała dynamikę sezonową, wyrażoną rocznym cyklem temperatury na różnych głębokościach gleby na obu stokach. Druga składowa wyraźnie różnicowała stoki, wskazując na utrzymującą się przez cały rok przewagę termiczną oraz większą akumulację ciepła poniżej głębokości 0,6 m na stoku o ekspozycji południowej. Uzyskane wyniki dowodzą, że profile termiczne gleb skutecznie odzwierciedlają zmienność mikroklimatyczną determinowaną ekspozycją stoków oraz stanowią solidne ramy do oceny zróżnicowania termicznego krajobrazu w skali lokalnej i regionalnej.